Icarus 215 (2011) 34–46

Contents lists available at ScienceDirect

Icarus

journal homepage: www.elsevier.com/locate/icarus

Impacts into non-polar ice-rich paleodeposits on Mars: Excess ejecta craters, perched craters and pedestal craters as clues to Amazonian climate history

Seth J. Kadish *, James W. Head

Department of Geological Sciences, Brown University, Providence, RI 02912, USA

ARTICLE INFO

Article history:
Received 22 February 2011
Revised 16 June 2011
Accepted 14 July 2011
Available online 23 July 2011

Keywords:
Mars, Surface
Mars, Climate
Ices
Impact processes
Cratering

ABSTRACT

We compare three previously independently studied crater morphologies – excess ejecta craters, perched craters, and pedestal craters – each of which has been proposed to form from impacts into an ice-rich surface layer. Our analysis identifies the specific similarities and differences between the crater types; the commonalities provide significant evidence for a genetic relationship among the morphologies. We use new surveys of excess ejecta and perched craters in the southern hemisphere in conjunction with prior studies of all of the morphologies to create a comprehensive overview of their geographic distributions and physical characteristics. From these analyses, we conclude that excess ejecta craters and perched craters are likely to have formed from the same mechanism, with excess ejecta craters appearing fresh while perched craters have experienced post-impact modification and infilling. Impacts that led to these two morphologies overwhelmed the ice-rich layer, penetrating into the underlying martian regolith, resulting in the excavation of rock that formed the blocky ejecta necessary to armor the surface and preserve the ice-rich deposits. Pedestal craters, which tend to be smaller in diameter, have the same average deposit thickness as excess ejecta and perched craters, and form in the same geographic regions. They rarely have ejecta around their crater rims, instead exhibiting a smooth pedestal surface. We interpret this to mean that they form from impacts into the same type of ice-rich paleodeposit, but that they do not penetrate through the icy surface layer, and thus do not generate a blocky ejecta covering. Instead, a process related to the impact event appears to produce a thin, indurated surface lag deposit that serves to preserve the ice-rich material. These results provide a new basis to identify the presence of Amazonian non-polar ice-rich deposits, to map their distribution in space and time, and to assess Amazonian climate history. Specifically, the ages, distribution and physical attributes of the crater types suggest that tens to hundreds of meters of ice-rich material has been episodically emplaced at mid latitudes in both hemispheres throughout the Amazonian due to obliquity-driven climate variations. These deposits likely accumulated more frequently in the northern lowlands, resulting in a larger population of all three crater morphologies in the northern hemisphere.

1. Introduction

The classification of crater and ejecta morphologies (Barlow et al., 2000) in the mid latitudes on Mars has led to the identification of three crater types that have been interpreted as impacts into an ice-rich surface layer. These morphologies include (Table 1): (1) Excess ejecta craters (EE), which are fresh craters that have anomalously voluminous ejecta deposits (Black and Stewart, 2008), (2) Perched craters (Pr), which include all craters that have their ejecta and crater interiors completely elevated above the elevation of the surrounding terrain (e.g. Boyce et al., 2005; Garvin et al., 2000; Meresse et al., 2006), (3) Pedestal craters (Pd), which have their crater interiors perched near the center of a plateau surrounded by an outward-facing marginal scarp (e.g. Barlow, 2005; Kadish et al., 2009).

Each of these morphologies has either ejecta or a pedestal that has a volume greater than that of the interior of the crater below the rim crest. Consequently, a formation mechanism has been proposed for each that involves the presence of a thick ice-rich surface unit at the time of impact, and the eventual preservation of parts of the ice-rich deposit via armoring of the surface or superposition of ejecta. When ice eventually sublimates from the intercrater terrain, most likely due to climate change from obliquity variations (e.g. Head et al., 2003; Levrard et al., 2004), the protective covering inhibits the loss of ice in the region proximal to the crater. This process lowers the elevation of the surrounding terrain, yielding craters that are either topographically perched or that have excessively voluminous ejecta.

The similarities between these morphologies and their proposed formation mechanisms suggest a potential genetic relationship

* Corresponding author.
E-mail address: Seth_Kadish@Brown.edu (S.J. Kadish).

0019-1035/$ - see front matter © 2011 Elsevier Inc. All rights reserved.
doi:10.1016/j.icarus.2011.07.014

Table 1
Commonly used abbreviations and respective definitions.

EE	Excess ejecta crater(s)	Fresh craters that have ejecta volumes above the pre-impact surface that are at least 2.5 times the volume of the crater cavity
Pr	Perched craters(s)	All craters whose current cavity floors and ejecta deposits are at or above the elevation of the surrounding terrain
Pd	Pedestal craters(s)	Craters characterized by having the crater interior located near the center of a pedestal that is surrounded by an outward-facing scarp
SLE	Single-layer ejecta	Ejecta consisting of only one layer of material
DLE	Double-layer ejecta	Ejecta consisting of two layers of material. The inner layer has a smaller diameter

among them. Although the crater types are not necessarily mutually exclusive form a morphological standpoint – many pedestal craters fit the technical definition of a perched crater – they do exhibit several key distinguishing features that may offer insight into the process of impacting into ice-rich material. In order to address these questions, we undertook new surveys and morphological analyses using recently released high-resolution images. Specifically, we discuss evidence for the possible genetic relationship among EEC, Pr, and Pd based on our new crater size, morphology, and geographic distribution database. In addition, using these new data, we identify and document the key similarities and differences in the characteristics of the three distinct crater types and assess the implications for their formation processes.

2. Morphological background

2.1. Excess ejecta craters

Excess ejecta craters (EE) are, by definition (Black and Stewart, 2008), fresh craters (Figs. 1 and 2). This criterion is established on the basis of the cavity depth and rim height of a particular crater, which must exceed specified cutoff values for a given region (Black and Stewart, 2008). In addition, EE have a distinct thermal inertia pattern in nighttime infrared images, with bright exposures (rocky material) on the crater walls, and a dark, low-thermal inertia signature from the unconsolidated ejecta material. By definition, EE have ejecta volumes above the pre-impact surface that are at least 2.5 times the volume of the crater cavity (Black and Stewart, 2008). Precise measurements of the ejecta volume are complicated by uncertainties in the profile of the structurally uplifted terrain on which the ejecta is superposed (Stewart and Valiant, 2006). As such, the value used for calculations includes the total integrated volume of the material above the pre-impact surface. This is compared to the volume of the pristine crater cavity below the elevation of the pre-impact surface. The ratio of these values, neglecting changes in the bulk density of the material, should be approximately equal to one. Using a set of fresh craters, Black and Stewart (2008) calculate the average V_{above}/V_{cavity} to be 0.99 with a standard deviation of 0.44. This means that, in order for a crater to be classified as an EE, its V_{above}/V_{cavity} value must be more than three standard deviations (3σ) from the mean (>2.5), completely separating it from the natural variability of typical fresh craters.

The initial survey for EE identified the highest concentration in Utopia Planitia (Black and Stewart, 2008). This survey was, however, geographically limited to 18–55°N, 86–163°E. Fresh craters from several smaller regions were used for morphological comparison, including part of Acidalia Planitia (27–54°N, 308–355°E). Classification of the ejecta revealed that EE tend to have double-layer ejecta (DLE) (Fig. 1), although examples with single-layer ejecta (SLE) exist (Fig. 2; Table 1). Barlow et al. (2000) define SLE craters as those surrounded by only a single layer of material. DLE craters are those surrounded by two layers of material, where the inner layer has a smaller diameter than the outer layer (Barlow et al., 2000). In either case, a morphological analysis of an EE ejecta deposit reveals minimal differences from that of normal ejecta; both normal and EE ejecta exhibit similar textures, and the margin of the outer layer ejecta merges relatively seamlessly with the topography of the surrounding plains. In some EE there exists a concentric topographic depression on the inner layer ejecta, just outside of the crater rim (Fig. 1). The EE measured by Black and Stewart (2008) range from ~5 to 18 km in diameter, although only craters from 4 to 50 km were included in the survey. The crater interiors, which may contain central peaks and pits, reach 600–1400 m depth below the elevation of the surrounding surface. Given the radii of the craters and the radial extents of the ejecta, the ejecta volumes correspond to excess thicknesses of 27–108 m (Black and Stewart, 2008).

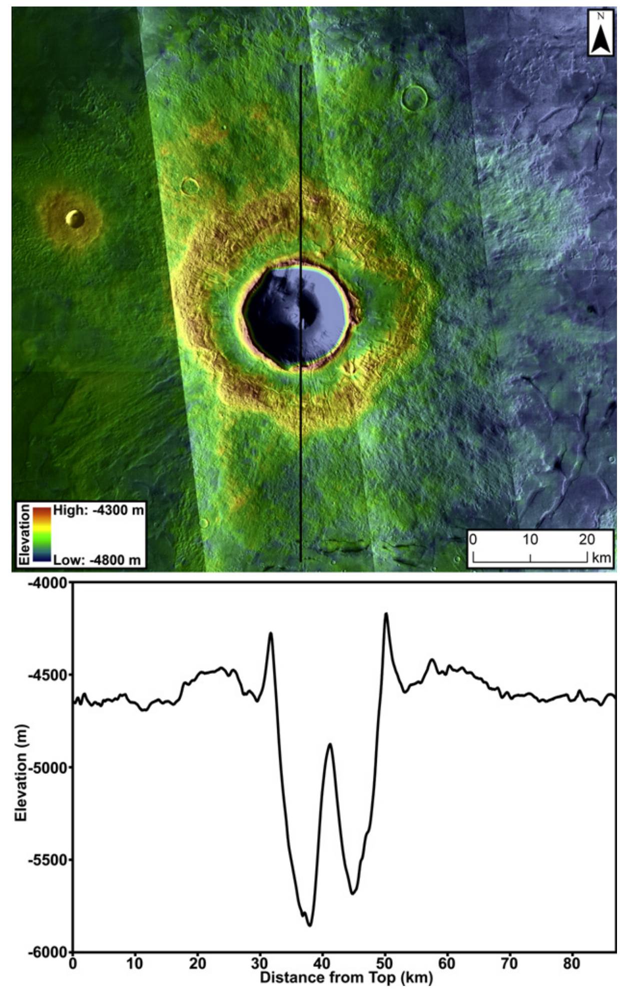

Fig. 1. An excess ejecta crater (EE) located at 38.5°N, 99.2°E, shown as a CTX mosaic with HRSC HiRes DTM data. The black north–south trending line across the crater shows the path of the topographic profile beneath the image, which has a vertical exaggeration of 30×. This EE, which has a V_{above}/V_{cavity} of 3.4, is 18.7 km in diameter, and the crater interior is approximately 1.2 km deep. The crater exhibits clear double-layer ejecta (DLE), with a moat-like depression directly outside of the crater rim. The outer layer of the ejecta is quite rough, making it easily distinguishable from the surrounding plains. The crater interior contains a prominent central peak, visible both in the image and topographic profile, derived from gridded MOLA data.

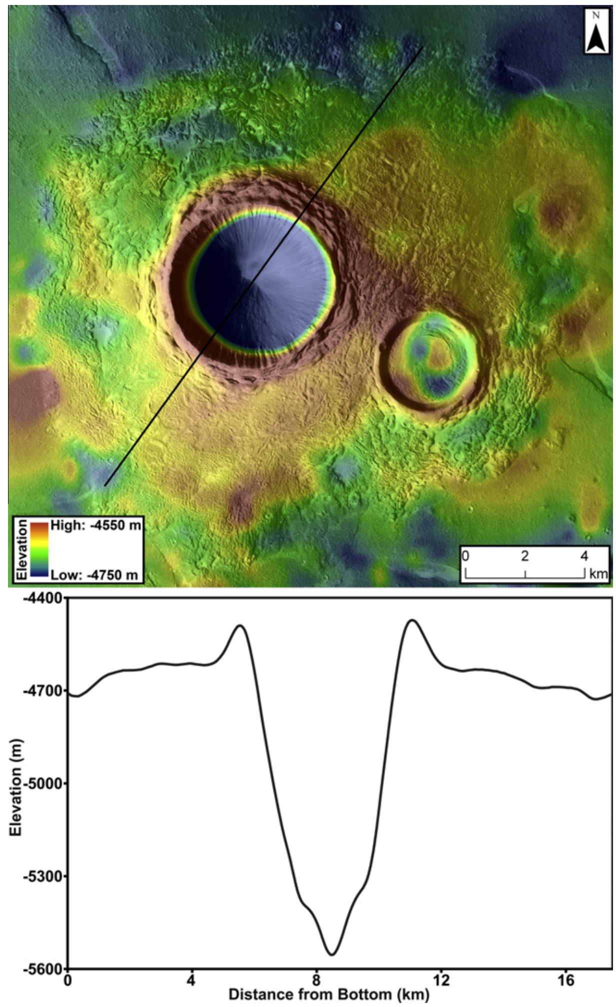

Fig. 2. An excess ejecta crater located at 32.8°N, 107.4°E, shown as a CTX mosaic with HRSC HiRes DTM data. The black SW–NE trending line across the crater shows the path of the topographic profile beneath the image, which has a vertical exaggeration of 10×. This EE, which has a V_{above}/V_{cavity} of 5.2, is 5.5 km in diameter and the crater interior is approximately 0.8 km deep. This fresh crater exhibits rough single-layer ejecta (SLE) that has a well-defined margin where it gently slopes down into the plains. The crater interior shows only minor evidence of infilling. The second crater in the image has similar ejecta morphology and, although the crater rim looks quite young, the crater interior has been almost completely infilled. This crater qualifies as a perched crater. The proximity of these examples suggests that the Pr may have been infilled by the ejecta of the EE.

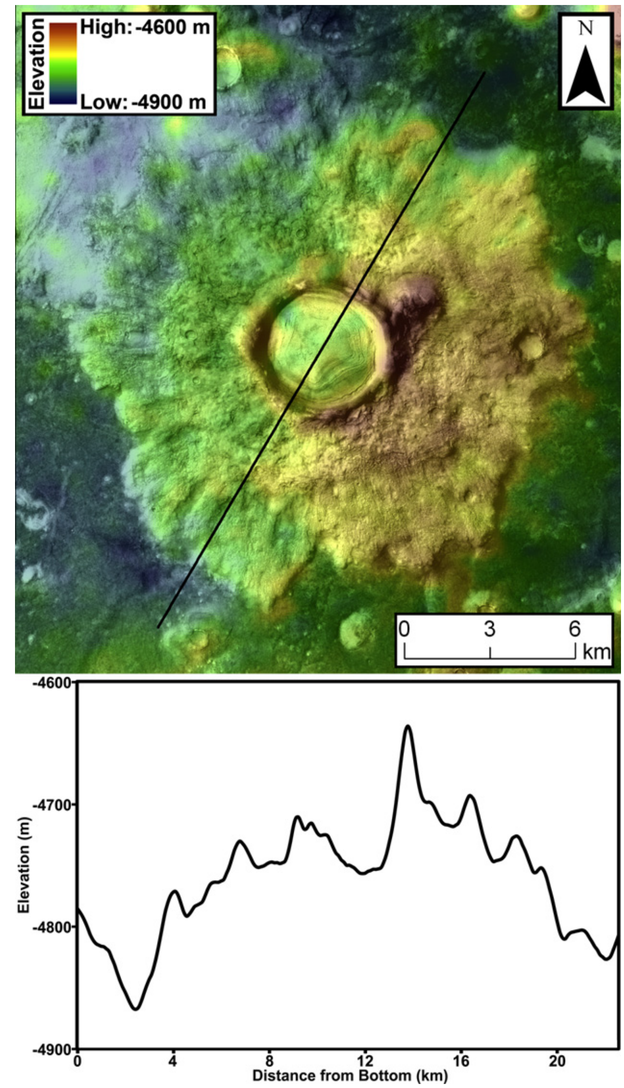

Fig. 3. A 4.3-km-diameter perched crater shown as a CTX mosaic with gridded MOLA topography. The black SW–NE trending line across the crater shows the path of the topographic profile, which has a vertical exaggeration of 51×. The crater interior exhibits clear concentric crater fill (CCF); due to the extensive infilling, the floor of the crater is now at the same elevation as the surface of the ejecta. The eastern half of the crater rim crest is still quite prominent, as can be seen in the image and the profile, but overall the rim appears to be considerably degraded. The ejecta, which itself contains small infilled craters, still has a distinguishable inner and outer layer. The radial striations are faintly visible, interrupted by the extremely rough surface texture. The margins of the ejecta are well-defined, creating a clear contrast with the relatively smooth surrounding plains.

2.2. Perched craters

The set of perched craters (Pr) includes all craters whose current cavity floors and ejecta deposits are at or above the elevation of the surrounding terrain (Boyce et al., 2005; Garvin et al., 2000; Meresse et al., 2006) (Figs. 3–5). These crater interiors have necessarily undergone significant infilling, decreasing the depths of the cavities; in extreme cases, the crater floor can be situated hundreds of meters above the intercrater plains. This process results in Pr having minimal variations in relief from the elevation of the surrounding plains to the lowest elevation of the crater floors (Boyce et al., 2005; Meresse et al., 2006). Through a survey of rectangular-shaped test areas (defined by the MOLA 1/128° DEM) in the northern lowlands, Boyce et al. (2005) found that Pr exist below an elevation of −2400 m. They tend to be located north of 40°N, although they are present as far south as 25°N, with the highest concentration in Utopia Planitia. Out of 2279 craters measured, Boyce et al. (2005) identified 414 examples of Pr with diameters ranging from ∼6 to 23 km. However, their study did not include craters smaller than 6 km in diameter. A subsequent study by Meresse et al. (2006) found several examples that were 3–10 km in diameter.

The ejecta and crater rims of Pr often show evidence of degradation or erosion (Figs. 3–5). The ejecta can be SLE or DLE (Barlow et al., 2000), and always exhibits a low thermal inertia in THEMIS nighttime images (Meresse et al., 2006). The texture of the ejecta is highly variable; it may be smooth or rough, and can exhibit radial lineations and/or pits. Measurements of the ejecta of Pr and normal DLE craters in Utopia Planitia have been used to estimate the excess thickness of the Pr ejecta, which is typically 60–80 m for the outer ejecta layer and 150–200 m for the inner ejecta layer. These ranges suggest an excess thickness of 35–140 m of material (Meresse et al., 2006). Despite Pr having inflated ejecta, the

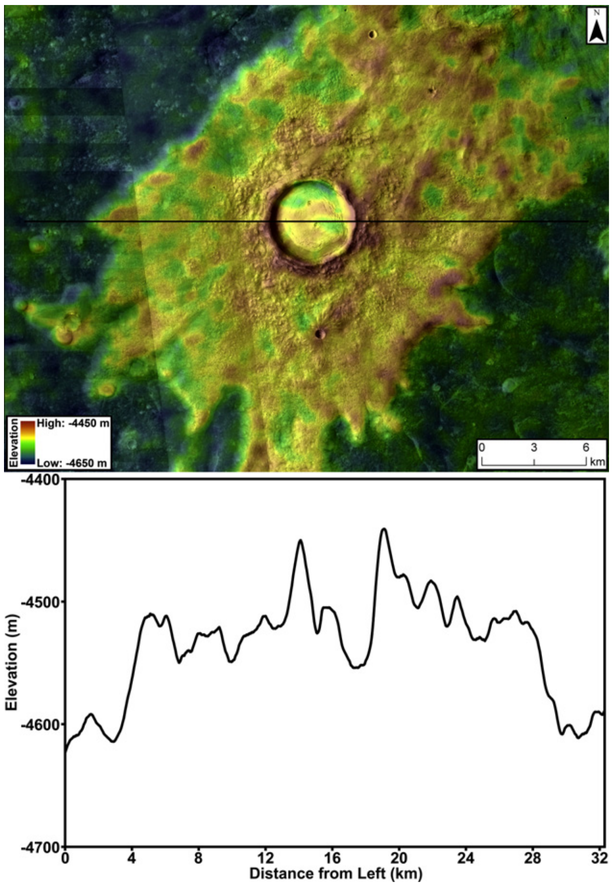

Fig. 4. A 4.8-km-diameter perched crater, shown as a CTX mosaic with HRSC HiRes DTM data. The black west–east trending line across the crater shows the path of the topographic profile, which has a vertical exaggeration of 73×. CCF has completely filled the crater interior, bringing the elevation of the crater basin level with the ejecta. The ejecta itself is DLE, with a rougher inner layer and a smoother outer layer that ends in a discontinuous rampart at its margin. Note that this ejecta is interacting with the ejecta of another crater to the northeast.

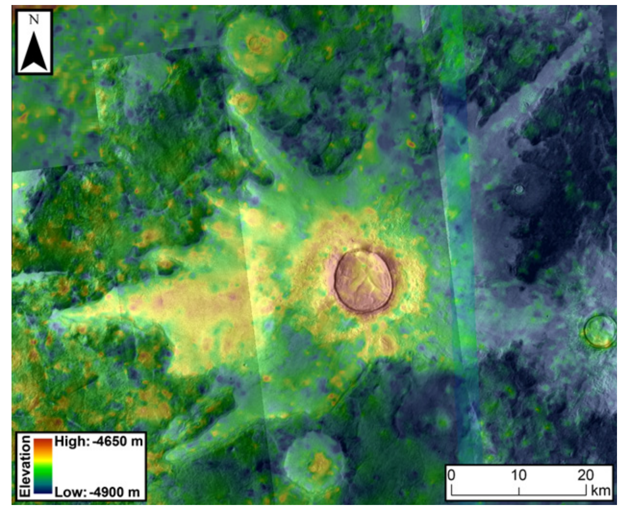

Fig. 5. A particularly interesting example of what could be classified as a heavily degraded 8.8-km-diameter perched crater, shown as a CTX mosaic with HRSC HiRes DTM data. The crater interior has undergone extensive infilling, and the fill material, which is heavily pitted, is now the highest part of the crater. Extensive sublimation/deflation of the ejecta is readily apparent, although both layers of the DLE can be identified, with slightly rougher texture on the inner layer. A moat-like pit, resembling scallops, extends around almost the entire margin of the outer ejecta, and is likely to be due to sublimation of the ice content of the ejecta. This sublimation and erosion is so advanced that, in some places where the plains have variable local topography, the ejecta is actually beneath the elevation of the plains. Other Pr/Pd are visible near the top and bottom of the image.

margins of the ejecta deposit usually slope gradually down to the elevation of the surrounding terrain, but do exhibit terminal ramparts in some cases. The material within the crater interiors is often concentric crater fill (Levy et al., 2010) (Figs. 3 and 4), but in some cases appears quite smooth with no evidence of cracks or flow. Additionally, the fill can be heavily pitted with depressions resembling scallops (Fig. 5), a feature interpreted to be due to sublimation (e.g. Lefort et al., 2009).

2.3. Pedestal craters

By definition, pedestal craters (Pd) are an impact morphology characterized by having the crater interior located near the center of a pedestal (mesa or plateau) that is surrounded by an outward-facing scarp (Barlow et al., 2000) (Figs. 6 and 7). The marginal scarp is generally located several crater diameters from the rim crest, which implies that the pedestal surface has a radial extent (Kadish et al., 2009) that exceeds that of a typical ejecta deposit (Barlow et al., 2000; Melosh, 1989). Some marginal scarps are marked by pits that represent loss of material from the pedestal; pit formation has been attributed to sublimation of the icy substrate below the protective veneer (Kadish et al., 2008) (Fig. 7).

Pd are generally small, with crater diameters less than 6 km (Fig. 6). The crater floors of mid-latitude Pd are usually but not always above the elevation of the surrounding terrain. In rare cases, the crater floor is above the elevation of the pedestal surface (Kadish et al., 2009) (Fig. 6A). Pedestals tend to be ~20–110 m in height. Although evidence of ejecta is uncommon, the pedestal surface can sometimes be superposed by SLE, which never reaches the pedestal margins (Kadish et al., 2010). A global survey revealed that the highest Pd concentrations are in Utopia and Acidalia Planitia, and Malea Planum (Kadish et al., 2009). For a more detailed description of the physical attributes and geographic distribution of Pd, see Kadish et al. (2008, 2009, 2010, 2011).

3. Formation mechanisms

The fundamental commonality among these three crater types is the interpretation that each morphology is the result of an impact into ice-rich surface deposits (Black and Stewart, 2008; Kadish et al., 2009; Meresse et al., 2006) (Fig. 8). As discussed in detail by Kadish et al. (2009, 2010), these ice-rich deposits must be similar to, but thicker than, recent icy mantling units that have been repeatedly emplaced at mid latitudes during periods of higher obliquity in the last several million years (e.g. Head et al., 2003; Kreslavsky and Head, 2002; Mustard et al., 2001).

Climate model results (e.g. Levrard et al., 2004; Madeleine et al., 2009) show that the necessary thicker deposits can accumulate over geologically-short time periods given the proper orbital and atmospheric conditions. These include an equatorial source of ice, such as the Tharsis tropical mountain glaciers (e.g., Forget et al., 2006; Head and Marchant, 2003), a moderate obliquity (35°), and high dust opacity. Variations on these constraints do change the quantity and geographic distribution of ice deposited at mid latitudes. However, Madeleine et al. (2009) show that accumulation rates can readily exceed 10 mm/yr at the same locations in which we identify the highest populations of EE, Pr, and Pd. Furthermore, the predicted history of martian obliquity variations during the past tens to hundreds of Myr (Laskar et al., 2004) suggests that the ice-rich material that leads to the formation of these crater morphologies is likely to have been emplaced episodically. This scenario would lead to multiple generations of ice-rich layers

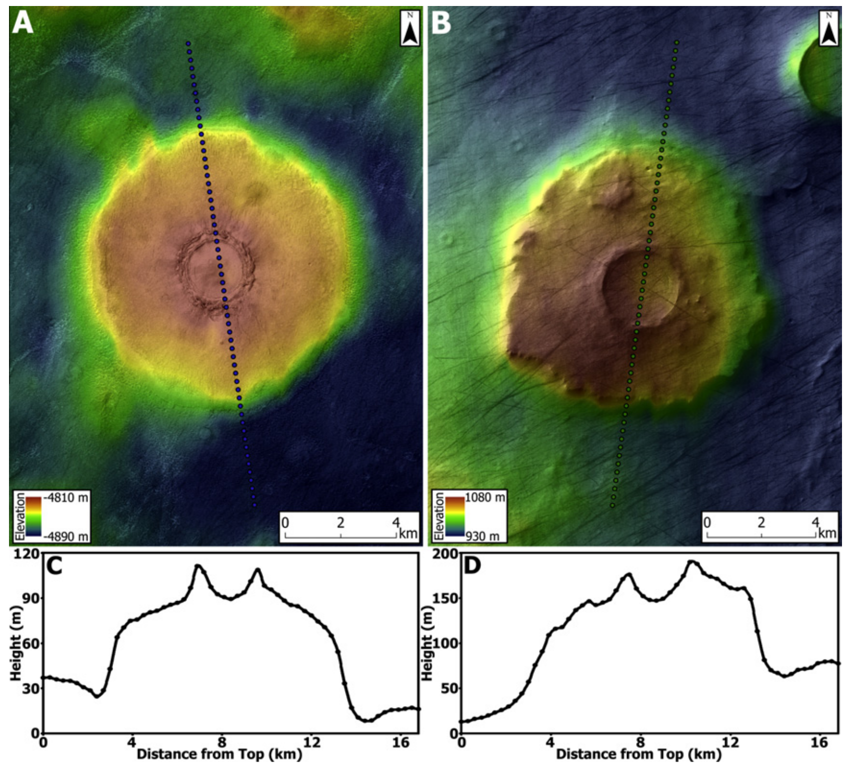

Fig. 6. Pedestal crater examples shown as CTX mosaics with gridded MOLA topography and corresponding profiles from MOLA shot data. Both of these craters show significant infilling of their crater interiors. Although they lack visible ejecta deposits, and both have a well-defined marginal scarp, which is a distinctive trait of Pd, by definition they both qualify as Pd. (A) A 2.1-km-diameter Pd located at 48.1°N, 101.3°E. (B) A 2.8-km-diameter Pd located at 57.2°S, 36.0°E. (C) A profile of the Pd in (A), showing the individual MOLA points. The vertical exaggeration of the profile is 67×. (D) A profile of the Pd in (B), showing the MOLA shot data. The vertical exaggeration of the profile is 40×. Modified from Kadish et al. (2010).

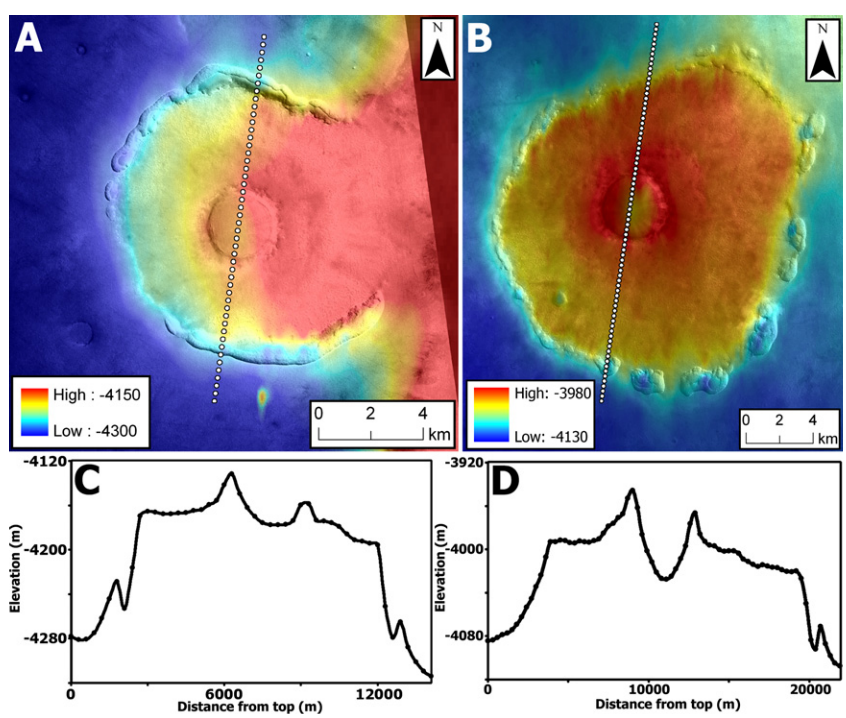

Fig. 7. Two examples of pedestal craters with marginal pits, shown as CTX mosaics with MOLA topography and corresponding profiles from MOLA shot data. Infilling of the crater interiors is visible in both cases. Neither crater shows clear ejecta on its smooth pedestal surface, but the topographic profiles reveal that both craters qualify as perched craters by strict definition. The marginal pits represent evidence of sublimation of ice from the pedestal material along the exposed scarps. (A) A 2.6-km-diameter Pd located at 60.2°N, 102.5°E. (B) A 3.9-km-diameter Pd located at 62.4°N, 99.4°E. (C) A profile showing the MOLA shot data of the Pd in (A). The vertical exaggeration of the profile is 44×. (D) A profile of the Pd in (B), derived from MOLA shot data. The vertical exaggeration of the profile is 67×. Modified from Kadish et al. (2009).

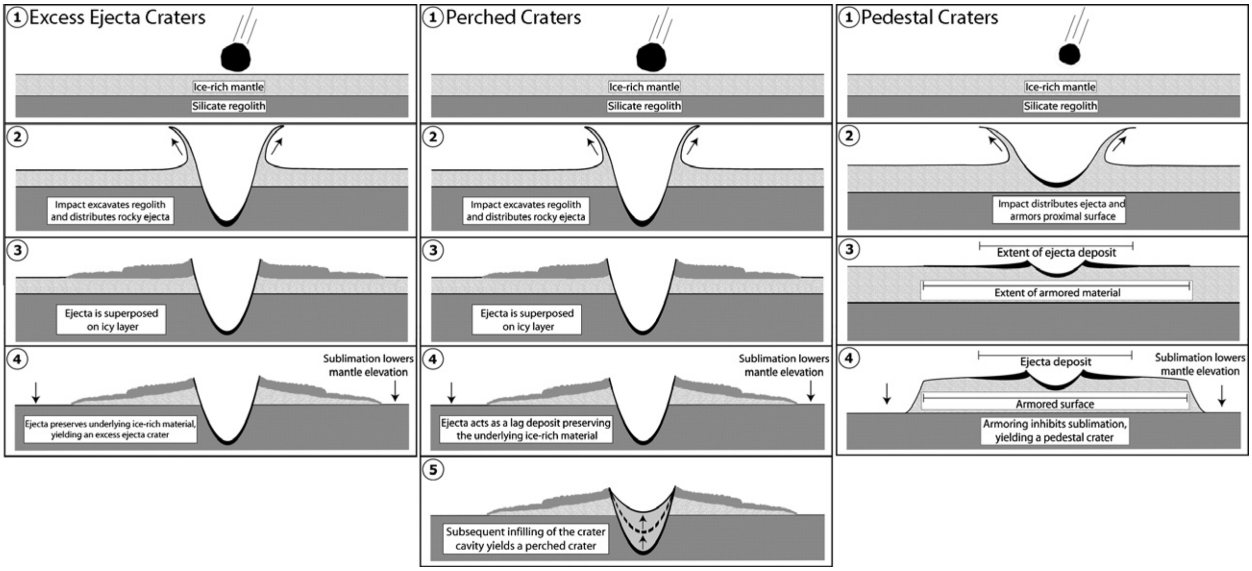

Fig. 8. Schematic illustrations highlighting the primary steps in the formation of excess ejecta craters (left), perched craters (middle), and pedestal craters (right). These process models for EE, Pr, and Pd have been adapted from Black and Stewart (2008), Meresse et al. (2006), and Kadish et al. (2009), respectively. Note the primary commonalities between the models, which include: (1) An impact into an ice-rich surface layer overlying the regolith. In the EE and Pr models, this impact completely penetrates through icy deposit to the underlying regolith, but this does not occur in the Pd model. (2) Sublimation/deflation of the ice-rich layer from the intercrater terrain, resulting in the lowering of the elevation of the surrounding plains. (3) Preservation of the icy layer proximal to the crater interior, either due to ejecta cover or related armoring processes. This results in the anomalously high volume of material around the crater in the form of excess ejecta or a pedestal. The only notable difference between the EE and Pr models is that, in the Pr model, the crater interior becomes infilled to the point that the floor of the basin is above the elevation of the surrounding terrain.

that were tens of meters thick, and to the production of these crater types upon impact of projectiles into this substrate, which is consistent with our observations (Kadish et al., 2010; Kadish and Head, 2011). Further, this sequence of events is necessary in order to maintain the presence of EE, which lose their classification as EE upon significant degradation or burial by mantling.

Formation mechanisms for EE, Pr, and Pd have been proposed on the basis of their topography, morphology, and distribution. The specific process models for EE, Pr, and Pd, which have been schematically detailed by Black and Stewart (2008), Meresse et al. (2006), and Kadish et al. (2009) respectively (Fig. 8), each begin with an ice-rich unit overlying a silicate regolith. This ice-rich material is interpreted to be the result of obliquity-driven climate change, and the redistribution of polar ice to lower latitudes (Head and Marchant, 2009). In the EE model, the ejecta, which is a mixture of ice and the underlying regolith, is distributed over the icy layer surrounding the crater cavity (Fig. 8A). During return to lower obliquity, the ice from the intercrater terrain sublimates, and the remaining dusty lag deposit is susceptible to erosion. The silicate-rich ejecta deposit, however, preserves the ice-rich layer surrounding the crater by insulating the ice fraction and inhibiting sublimation (Black and Stewart, 2008; Kadish et al., 2009; Meresse et al., 2006). Consequently, the terrain surrounding the ejecta is lower than the surface was at the time of impact, so that the ejecta appears thicker than expected. The excess ejecta may be composed purely of a sublimation lag deposit left from the former icy substrate, or it may also contain some fraction of the original ice (Black and Stewart, 2008).

The model for Pr formation proposed by Meresse et al. (2006) follows a sequence similar to that interpreted to have occurred during the production of EE (Black and Stewart, 2008), beginning with an impact that penetrated an ice-rich deposit superposed on a silicate-rich regolith and excavated the regolith material. The resulting lobate ejecta is distributed in the region proximal to the crater rim crest and interior, on top of the ice-rich layer. In their process model, Meresse et al. (2006) propose that, after impact, the crater interior acts as a trap for debris, and is slowly infilled by the eolian transport of material, as well as by nearby impact ejecta and possible deposition from the atmosphere; this aspect of the model has yet to be tested using quantitative modeling. Meresse et al. (2006) claim that, if the crater is sufficiently small, the infilling will raise the elevation of the crater floor above the elevation of the surrounding terrain. Meanwhile, thermal variations and wind deflation respectively sublimate and erode the icy surface layer. The changes in temperature may be due to orbital changes (i.e. eccentricity and obliquity) and/or seasonal effects. The Pr ejecta deposits, however, have low thermal inertia (Meresse et al., 2006), possibly due to a thin insulating layer of fine-grained material. As a result, the ejecta is preferentially protected from the thermal fluctuations, helping to preserve the ice content of the ejecta. Although the ejecta itself is also subject to eolian erosion, it is removed at a much lower rate than the intercrater plains. The result is a crater that has both its ejecta and crater interior perched above the surrounding terrain (Meresse et al., 2006).

In the general proposed Pd formation model (Kadish et al., 2009), an impact occurs into a layer of ice and snow, mixed with dust, but the excavation cavity does not necessarily reach the underlying silicate regolith. The impact event distributes ejecta and possibly impact melt on and around the crater rim; due to the composition of the target material, the ejecta itself is likely to be largely ice and snow. The surface proximal to the crater becomes indurated in some manner as a result of the impact process (Arvidson et al., 1976; Osinski, 2006; Schultz and Mustard, 2004; Skorov et al., 2001; Wrobel et al., 2006). The resulting armored surface can extend to a distance of multiple crater radii, exceeding the lateral extent of the ejecta deposit. Subsequent obliquity-driven climate change leads to the sublimation of volatiles from the unarmored intercrater terrain, lowering the elevation of the plains. The armoring, however, inhibits sublimation from beneath the hardened pedestal surface. This produces a symmetrical, circular scarp around the edge of the armored crater and its ejecta. The result is a crater centered on a pedestal that is composed of the initial icy layer that was deposited on the silicate regolith. In this model, the crater interior is usually above the elevation of the surrounding terrain, and infilling of the crater interior can occur, raising the elevation of the crater above that of the pedestal surface (Kadish et al., 2009).

It should be noted that other models for Pd formation have been proposed (e.g. Arvidson et al., 1976; McCauley, 1973). These studies suggested that Pd resulted from impacts into dry, fine-grained material. An armoring mechanism indurated the proximal surface, allowing eolian deflation to remove the nonarmored intercrater terrain while preserving the pedestal material. This left the Pd perched above the surrounding plains (Arvidson et al., 1976; McCauley, 1973). In both the ice-rich and dry models, a host of armoring mechanisms have been proposed. These include increased ejecta mobilization caused by volatile substrates (e.g. Osinski, 2006), a coarse lag deposit (Arvidson et al., 1976), a veneer of impact melt (Schultz and Mustard, 2004), dust insulation (Skorov et al., 2001), or a thermally indurated soil consisting of a layer of fine-grained, volatile-poor dust and/or salts (Wrobel et al., 2006). For a discussion of these armoring mechanisms, see Kadish et al. (2009).

In comparing this range of characteristics and these proposed formation mechanisms, it is clear that the processes may be similar, particularly between EE and Pr. In both of these cases, the initial impact excavates the underlying regolith, and the distributed ejecta is primarily responsible for inhibiting the sublimation of the proximal volatiles during erosion of the intercrater terrain, leading to the anomalously large ejecta volumes. The only significant distinction between the geomorphological outputs identified in the process models is the infilling of the crater interiors; all EE are necessarily fresh, having deep crater cavities, whereas Pr have always undergone extensive infilling, yielding shallow crater interiors. Pr are also more likely to show modification of their ejecta deposits, possibly due to eolian deflation (Meresse et al., 2006). As will be discussed later, this may imply that Pr are simply modified EE which have been degraded and/or covered by post-emplacement deposits.

Based on the limited extent of Pd ejecta deposits, which are not always present on the pedestal, it is very likely that Pd have experienced a different process by which the ice-rich material becomes preserved. As previously mentioned, several mechanisms have been proposed that could be capable of armoring such a large surface area relative to the size of the crater interior, but none have been proven (Arvidson et al., 1976; Osinski, 2006; Schultz and Mustard, 2004; Skorov et al., 2001; Wrobel et al., 2006). The absence of ejecta associated with many Pd supports the interpretation that the impacts that form Pd, unlike EE and Pr, do not excavate a significant volume of the underlying silicate regolith. As such, the ejecta would consist primarily of the ice-rich layer, making it easily erodible, and would have a very small rock fraction. This observation argues against armoring mechanisms that rely on rocky ejecta to armor the pedestal surface, which include the hypotheses of ejecta mobilization (Osinski, 2006), lag deposits (Arvidson et al., 1976), and impact melt (Schultz and Mustard, 2004).

Using the depth-diameter relationship for simple craters of $d = 0.21D^{0.81}$, where d is the transient depth and D is the diameter (Garvin et al., 2003), and the approximation that excavation depth is one-third of the transient depth (Melosh, 1989), it is clear that the impacts resulting in Pd (1–3 km diameter craters) tend to excavate only 70–170 m. This produces transient crater depths from 200 to 500 m below the rim crest. These depths will vary due to the strength of the impact target material (Garvin et al., 2000). Because the impact excavation depth is comparable to the thickness of material that is eventually removed due to sublimation and deflation, most Pd have their crater basins and any detectable ejecta perched above the elevation of the intercrater plains. By strict definition, this would allow them to be classified as Pr. However, as we will emphasize in the following section, while some Pd may technically qualify as Pr, the two morphologies are not identical, having several distinguishing physical and topographic features.

4. Physical attribute comparison

4.1. Crater diameter and ejecta/pedestal thickness

One of the significant physical distinctions between these crater types is the variation in diameter ranges (Fig. 9). As previously mentioned, the initial studies of EE and Pr revealed that they tend to be approximately the same size range. Although these studies did not survey craters of all diameters, the distribution of sizes in confirmed examples suggests that the majority of EE and Pr are between 4 and 10 km in diameter, with extreme cases extending the range from 2 to 23 km (Black and Stewart, 2008; Boyce et al., 2005; Meresse et al., 2006). Conversely, Pd typically range from <0.5 to 6 km in diameter, with a median of 1.2 km (Kadish et al., 2009). These distributions show that the lower size limit for EE and Pr overlaps only slightly with the upper size limit of Pd (Fig. 9). As such, if all three crater types form from impacts into the same icy paleodeposits, then this distinction in crater sizes suggests that the primary factor influencing the initial morphology of the observed craters is the excavation depth (Barlow et al., 2001), which scales with the total impact energy based on the size and velocity of the impactor.

The validity of the above assumption relies on the notion that each crater type results from distinct impacts into the same thickness of ice-rich paleodeposits, rather than being produced by impacts into deposits of different thicknesses that were present at different times. To assess this, we can compare the thicknesses of the excess ejecta, perched ejecta, and pedestals (Fig. 9). If these morphologies do form from the same icy layers of the same thickness, then their proposed formation mechanisms predict that the ejecta/pedestals will have similar thicknesses.

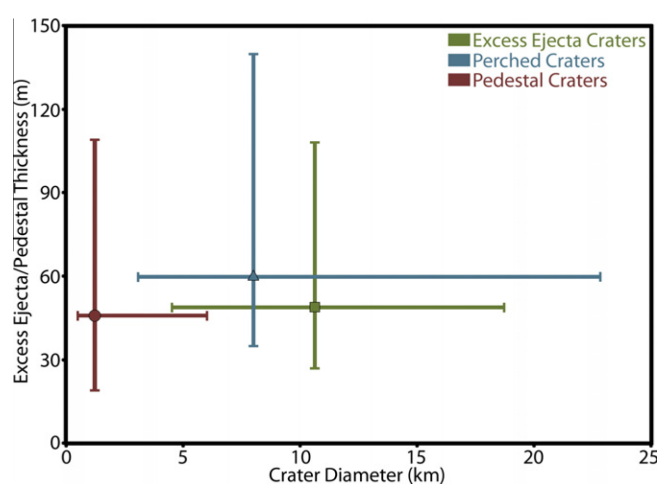

Fig. 9. A graph of the crater diameter and thickness values for EE (green square), Pr (blue triangle), and Pd (red circle). Locations of the data points show the approximate average values for each crater population while the error bars indicate the range of values, as identified by Black and Stewart (2008), Boyce et al. (2005), Meresse et al. (2006), and Kadish et al. (2009). These data exclude extreme cases – for example, the new EE found in this study show that some examples can be much smaller in diameter than the population identified by Black and Stewart (2008). This visualization of the typical physical characteristics the crater morphologies clearly shows the similarity between their thicknesses (vertical error bars). The diameters (horizontal error bars) show that there is an overlap between larger Pd and smaller EE and Pr, but Pd tend to be smaller while EE and Pr are similar in size. (For interpretation of the references to colour in this figure legend, the reader is referred to the web version of this article.).

As previously mentioned, Black and Stewart (2008) found that EE range from 27 to 108 m in excess thickness based on the expected thickness of the ejecta for a given crater size. They identified a mean excess thickness of approximately 50 m. In their study of Pr, Meresse et al. (2006) noted that the DLE of an average Pr is 35–140 m thicker than that of a normal crater. Lastly, Kadish et al. (2010) showed that the vast majority of the pedestals of Pd are 20–110 m in thickness, with a mean of 46 m. These measurements were made on the pedestal, but outside of the outer margins of any visible ejecta, so they act as a proxy for the thickness of the icy paleolayer, comparable to the physical significance of the excess ejecta measurements for EE and Pr (Kadish et al., 2010). The similarity of the thicknesses of each of the three morphologies is remarkable (Fig. 9); these results strongly support our interpretation that EE, Pr, and Pd all formed from impacts into ice-rich deposits of similar thicknesses. Furthermore, these data suggest that the deposits were, on average, several tens of meters thick, and in some cases exceeded 100 m in thickness.

This finding may also explain the apparent lack of EE and Pr larger than 20 km. Boyce et al. (2005) note that Pr larger than 10 km in diameter would not be common due to the difficulty of completely infilling such a voluminous cavity. This, however, would not affect the size range of EE, which have not been identified larger than 18 km in diameter despite the fact that Black and Stewart (2008) extended their survey of fresh craters up to 50 km in diameter. From a process perspective, given the method by which EE and Pr are interpreted to have formed, a size limitation imposed by the thickness of the icy target layer would be expected. Because the ice-rich deposit has a fixed thickness, the volume of excess ejecta will become proportionately smaller as the fresh crater size increases. This will reduce the V_{above}/V_{cavity} ratio below the necessary 3σ value of 2.5 required for EE classification. Additionally, it is likely that the heat generated from larger impacts would more completely melt the volatile fraction of the proximal icy layer upon impact, further reducing the proportion of excess ejecta. This melting has been shown to occur for Sinton crater, a large impact that is interpreted to have formed on a plateau icefield (Morgan and Head, 2009). Essentially, large impacts resulting in craters greater than about 25 km would overwhelm the tens of meters of ice-rich material at the surface, resulting in a negligible change to the ejecta volume.

4.2. Topography and morphology of ejecta

A second apparent distinction between these three crater types is the texture and topographic profile of their ejecta (Figs. 1–7). Both in images and in profile, the ejecta of EE closely resembles that of typical crater ejecta (Garvin et al., 2000); without supporting volumetric measurements of the ejecta and crater interior, it would be extremely difficult to distinguish an EE from a normal fresh crater with DLE (Figs. 1 and 2). The typical DLE of EE slopes gradually downward from the well-defined crater rim crest, with the steepest slopes occurring in the transition between the inner and outer layers of the ejecta. As previously mentioned, some EE exhibit a concentric topographic depression on the inner layer ejecta bordering the crater rim crest. This moat-like trait is typical of most DLE, and is interpreted to be a primary feature resulting from the supersonic nature of the outward flow responsible for producing the inner ejecta layer (e.g. Boyce and Mouginis-Mark, 2006). Topographically, the outer ejecta layer merges almost seamlessly with the surrounding plains. However, images of EE ejecta usually exhibit rough textures and often reveal surfaces that have clear radial striations. This characteristic roughness contrasts sharply with the smooth texture of the plains in Utopia (Figs. 1 and 2).

The ejecta of Pr is similar to that of EE, with a few notable distinctions. Similar to the crater interior associated with Pr, the ejecta often shows evidence of having been covered by debris. Although the texture maintains a rough appearance, which is confirmed in the topographic profiles, it is usually somewhat more subdued than that of the fresh ejecta associated with EE, as are the radial striations that are present on most Pr ejecta (Figs. 3–5). Unlike EE ejecta, Pr ejecta sometimes has a terminal rampart, especially in DLE cases. The ejecta of most Pr, however, gradually slopes down to the surrounding plains. This is always the case in SLE examples of Pr. Topographic profiles of Pr can give the false impression that Pr ejecta is quite distinct from EE ejecta. This interpretation of the ejecta is influenced by the absence of a deep crater interior and an eroded crater rim, which in some cases makes the ejecta difficult to distinguish from the crater. Variations in vertical exaggeration (Figs. 1–7) also make Pr ejecta appear deceptively rough when compared to EE ejecta. Morphological assessments, however, suggest that Pr ejecta most often represents a subdued/degraded version of EE ejecta. It should be noted that, despite these common differences between Pr and EE ejecta, the two can sometimes be practically indistinguishable; in these cases, Pr appear to be EE with a filled-in crater interior (Fig. 2).

A detailed discussion of typical Pd ejecta is difficult because the presence of ejecta on the pedestal surface is so uncommon. When SLE is present, it is almost always thin, contributing only a slight halo of roughness to the otherwise smooth flat pedestal surface (see Fig. 7 in Kadish et al., 2010). The texture of Pd ejecta is often so subtle that it is detectable only in high resolution (MOC, CTX, HiRISE) images, and even then its distal perimeter cannot always be distinguished from the pedestal surface. Topographic profiles of typical Pd are distinct when compared to EE and Pr in that Pd always have a well-defined scarp at the margin of their pedestal (Figs. 6 and 7). This scarp should not be confused with a characteristic of the ejecta, however, as the pedestal and ejecta are distinct features. Variations in elevation due to the presence of ejecta are difficult to discern using MOLA topography due to the $\sim$300 m spacing between data points (e.g. Smith et al., 2001). As such, Pd topographic profiles show that the pedestal is by far the most prominently expressed feature. Depending on the freshness of the Pd, the crater rim and crater interior may be well-defined like that of EE, or significantly subdued like that of Pr.

5. Age comparison

Superposed impact crater size–frequency distributions can be used to estimate the ages of craters and their ejecta deposits, despite small sample sizes and counting areas. Crater counting on the ejecta/pedestal of EE, Pr, and Pd can provide estimates of the ages of individual craters. If this method is repeated on many distinct small surfaces, it is possible to produce a preliminary age range. In addition, preservation states can be used to make inferences about the relative ages of crater populations. It is therefore useful to provide a general description of age estimates for the populations in order to place the formation mechanisms within the context of the climate history of Mars. In this section, we provide crater counts on ejecta for individual crater ages, as well as lower limits for population ages; calculating the age of a crater population using the conventional size–frequency distribution technique is difficult because the method dates the age of the surface, which is not necessarily the individual crater formation age. However, using the diameters of a crater population and the area on which it is present will yield the minimum duration of time necessary to form that population.

Black and Stewart (2008) calculate the apparent retention age of their fresh crater population in Utopia to establish that the EE population has an apparent age of 100–200 Myr. It should be noted that this is not the age of any specific crater, but rather the time interval required to form the EE population when the necessary icy deposit was emplaced. The time needed to form the observed population is necessarily greater than ~200 Myr because the ice-rich material is not currently present and a robust solution for the last 20 Myr of martian obliquity history shows low obliquity periods for the last 3–5 Myr, and potentially widely variable obliquity for the last 250 Myr (Laskar et al., 2004). Given the rarity of EE – only 10 of the 572 fresh craters measured by Black and Stewart (2008) qualified – and the 200 Myr formation timescale, Black and Stewart (2008) suggest that EE production is associated with an episodic phenomenon. They conclude that EE ages are likely to have spanned the Amazonian period, forming in conjunction with multiple distinct ice-emplacement episodes, and that the fresh appearance of EE supports the interpretation that they are young (Black and Stewart, 2008).

The dating of Pr is complicated by the fact that the ejecta deposits have undergone noticeable modification, including mantling, burial and morphologic degradation. If the crater interior has been filled by a significant volume of sediment, then it is reasonable to believe that material has also accumulated on the ejecta deposits. This process also infills and erases craters, leading to the calculation of artificially young ages. Because of this, the age range of Pr is not well defined. Their degraded states strongly imply that they are older than EE. Boyce et al. (2005) used stratigraphic relationships between Pr and the Vastitas Borealis Formation to determine that Pr are likely Late Hesperian or Early Amazonian in age.

The timescale of formation of Pd was calculated using the mid-latitude Pd population and the corresponding area on which they formed. Similar to the EE time interval, this method leads to a derived formation timescale of approximately 100 Myr (Kadish et al., 2009). Using the same logic outlined for the accumulation of EE, this result implies that Pd are likely to have formed throughout the Amazonian during episodic periods of mid-latitude ice-rich deposits. The episodic emplacement of Pd has also been confirmed by stratigraphic relationships in which one Pd is partially draped over another Pd (Kadish et al., 2010). Additional work on dating 50 individual pedestal surfaces revealed that 70% of those measured are younger than 250 Myr. These individual ages are, however, lower-limit calculations due to modification and resurfacing of the pedestals. In addition, 20% of the pedestal surfaces were calculated to be more than 1 Gyr in age. These examples appear significantly more degraded, and show evidence of infilling of their crater interiors, similar to the morphology of Pr.

The combination of these dating efforts for each of the three crater types provides a general timeline for their formation. The probable recurrence of the ice-rich paleodeposit from which EE, Pr, and Pd form suggests that none of the populations resulted from a single phase. In addition, multiple crater types may have formed from the same phase. Despite these possible overlaps and extended formation timescales, it is likely that Pr are generally the oldest of the three morphologies. Pr consistently display the most degradation, and the observation that some show partial burial by the Vastitas Borealis Formation implies a Hesperian age. Pd appear to be generally young (tens to a few hundred Myr), but some individual examples show that they can be much older (a few Gyr). As a population, EE are necessarily fresh and are likely to be the youngest of the crater types.

6. Geographic distribution comparison

The initial survey for EE by Black and Stewart (2008) noted that, within the study region, nine of the 10 EE identified were located in Utopia Planitia (Fig. 10). The only other EE was located in Acidalia Planitia. Black and Stewart (2008) also identified nine moderately excess ejecta craters (MEE), with $V_{\text{above}}/V_{\text{cavity}}$ between 2 and 2.5, five of which were in Utopia, three in Acidalia, and one in Isidis. Due to the common modification of craters near the poles from mantling, high latitudes were not included in the study. As such, the limited latitudinal range at which EE were identified, primarily between 32°N and 44°N, is not a comprehensive assessment of the distribution of EE. Black and Stewart (2008) specifically note that it is likely that other EE have formed in their study region, but have subsequently been modified and/or degraded, and that many EE may exist outside their survey area.

Surveys detailing the distribution of Pr also covered regions exclusively in the northern hemisphere (Boyce et al., 2005; Meresse et al., 2006). These studies found that the highest concentrations of Pr are in Utopia, Acidalia, and Arcadia Planitia between 40°N and 55°N (Fig. 10), but they have been identified as far south as 25°N. Given the sheer number of confirmed Pr – 414 in the limited survey area of Boyce et al. (2005) – it is clear that they are significantly more common than EE. Fig. 10 shows that both Pr and EE are most heavily concentrated in Utopia and somewhat less so in Acidalia, with only Pr being present in Arcadia. As we will show in the following section, both EE and Pr are present, but less common, in the southern hemisphere of Mars.

The distribution of more than 2300 Pd larger than 0.7 km in diameter has been well established between 60°S and 60°N (Kadish et al., 2009). This study shows that, like EE and Pr, the highest populations of northern hemisphere Pd are in Utopia and Acidalia. Pd are also concentrated in Arcadia (Fig. 10). Of the Pd measured, four times as many exist in the northern hemisphere than in the southern hemisphere. Those that are present south of the equator tend to be focused in Malea Planum, with much smaller populations in Terra Cimmeria and Terra Sirenum. Latitudinally, Pd extend as far equatorward as 33°N and 40°S. Subsequent high-latitude studies have confirmed that Pd are common near the poles, and can even form on the polar caps (Kadish and Head, 2011). These data confirm that, of the three crater morphologies, Pd are the most common and widespread (Fig. 10).

7. New examples of excess ejecta craters

Due to the geographic limitations of previous surveys for EE and Pr, as outlined in Section 2, we expanded the search for these crater morphologies into the southern hemisphere. This was necessary in order to provide a more complete geographic comparison of the locations in which EE, Pr, and Pd are capable of forming, an observation that is a key aspect of understanding the relationship between the crater types. We performed a survey from 0° to 70°S using a THEMIS IR mosaic and MOLA altimetry. The combination of images and topography allowed us to select fresh craters, as well as some that had both the crater interior and ejecta perched above the surrounding plains.

Fresh craters with clear ejecta were generally included down to 2 km in diameter unless good quality CTX coverage was available, and then we were able to measure some smaller examples. This cutoff was necessary because, without high resolution images of small craters, it is not possible to confirm that they are fresh. Some craters that would classify as both Pr and Pd were previously identified in the southern hemisphere from the Kadish et al. (2009) survey for Pd. We expanded the search for new examples of Pr that would not be classified as Pd. Overall, our analysis revealed that EE, like Pd, are much rarer in the southern hemisphere, and Pr are similarly uncommon.

Using high resolution HRSC DTMs (50–150 m/pix resolution) and 1/128 degree gridded MOLA data (463 m/pix), we created eight profiles of each fresh crater we studied. This was done to identify and compensate for outliers. Although these two datasets have significantly different resolutions, they produced remarkably

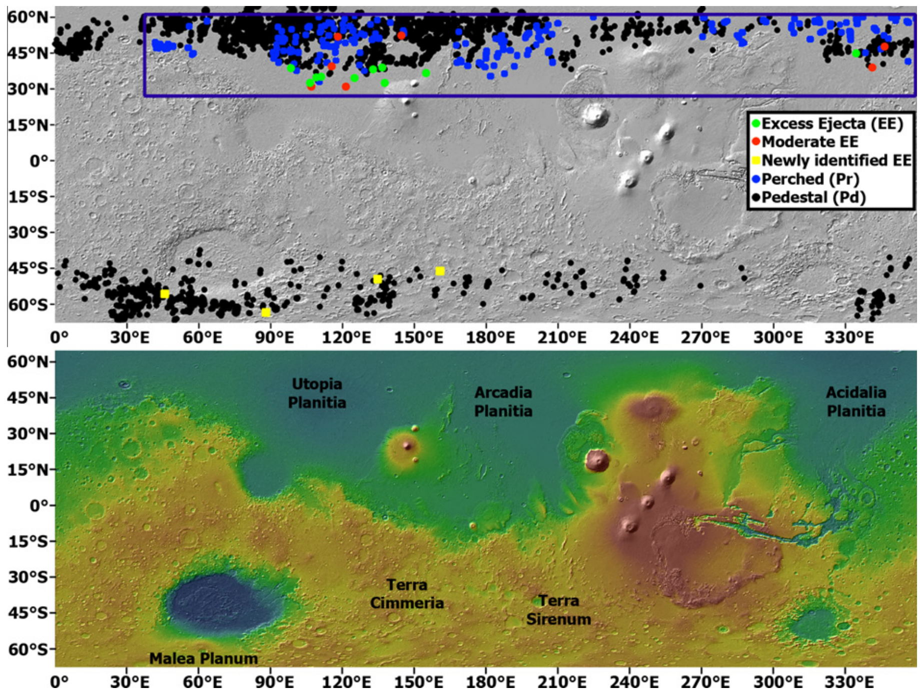

Fig. 10. The top map shows the geographic distribution of excess ejecta craters (green dots) and moderately excess ejecta craters (red dots) from Black and Stewart (2008), perched craters (blue dots) from Boyce et al. (2005), pedestal craters (black dots) from Kadish et al. (2009), and newly identified excess ejecta craters in the southern hemisphere (yellow squares). The bottom map, which shows MOLA topography, identifies significant regions of interest. Due to the limited geographic extent of previous surveys for EE and Pr, we have outlined the general region over which they were identified with a purple box. Note, however, that neither the EE nor the Pr survey included the entire area of the purple box; the EE survey covered only 86–163°E and 308–355°E for the latitudes shown (Black and Stewart, 2008), while the Pr survey was limited to distinct rectangular regions based on the available MOLA 1/128° DEM (Boyce et al., 2005). In addition, both the EE and Pr studies ignored craters smaller than 4 and 6 km in diameter, respectively. Despite these limitations, the distribution shows clear similarities in where EE, Pr, and Pd form, with the highest concentrations in Utopia and Acidalia Planitia, and the new southern hemisphere EE are all located in regions where Pd are present. In terms of population density, these data show that Pd are the most widespread, while EE are the least common. (For interpretation of the references to colour in this figure legend, the reader is referred to the web version of this article.).

similar profiles. We then detrended the profiles by subtracting the regional topographic slopes, which we derived from profiles of the plains surrounding the craters to a distance of at least 15 km beyond the extent of the ejecta deposits. These linear slopes were interpolated over the crater basin to establish the elevation of the pre-impact surface at the point of impact. Averaging these profiles for each individual crater allowed us to measure the crater depth and width and the average excess ejecta thickness. Crater depths were confirmed using MOLA shot data. It should be reiterated that, in this case, crater depth refers to the difference in elevation between the surrounding plains and the deepest point of the crater basin, and is not dependent on the crater rim height. We then measured the areal extent of the ejecta and multiplied this by the average excess ejecta thickness to get the excess ejecta volume (V_{ejecta}). To calculate the crater volume (V_{cavity}), we ran a best-fit algorithm on the averaged crater profiles, allowing it to select from a hyperbolic, conic, or parabolic (power law) equation. In each case, the best-fit was a parabola with a correlation coefficient of >0.98. The resulting equation was then rotated around the z-axis to create a paraboloid, and integrated according to the depth of the crater. We also tested HRSC DTM profiles and gridded MOLA profiles separately to ensure that differences in dataset resolution had no bearing on our results. The HRSC and MOLA profiles always yielded volumetric measurements within 2% of each other; this degree of error is trivial in determining whether the examined fresh craters qualify as excess ejecta craters. Using these values, we were able to confirm the presence of four craters with V_{cavity}/V_{ejecta} greater than 2.5 (Fig. 11 and Table 2). It should be noted that, by using the techniques set forth by Black and Stewart (2008), we assume that the typical V_{cavity}/V_{ejecta} is not significantly different for craters in the southern hemisphere, and thus a value of 2.5 is still 3σ from the average.

Interestingly, no EE were identified that had a diameter greater than 3 km (Table 2). Because Black and Stewart (2008) only measured fresh craters larger than 4 km, these new EE are considerably smaller than those previously analyzed. There is, however, one EE of comparable size, named Vaduz, which has been analyzed in detail by Schaefer et al. (2011). Because these craters are so small, they are readily susceptible to erosion. As such, the rarity of their presence, having survived the sublimation and removal of the surrounding ice-rich target layer, is not surprising. The new EE, in addition to having small diameters, also have relatively thin excess ejecta (16–26 m) compared to measurements by Black and Stewart (2008). The ejecta of these EE examples is always of the DLE type and is remarkably extensive compared to the sizes of the craters (Fig. 11). The small volumes of the crater cavities and large extents of their ejecta yield high V_{cavity}/V_{ejecta} values, reaching up to 28.5 (Table 2). Unlike the northern hemisphere examples, these EE appear to have relatively smooth ejecta, although this interpretation may be hindered by limitations of the image resolution; some portions of the ejecta do appear rougher than others, and there are signs of sublimation pits on the surface of at least one of the new EE ejecta deposits (Fig. 11A).

The newly identified EE are located exclusively between 45°S and 65°S, and are all in the eastern hemisphere, which is where the vast majority of southern hemisphere Pd are located (Fig. 10). These EE are not, however, within close proximity of each other. Each is located in or near a Pd field (within hundreds of km), and we have identified one example that is only tens of km from two Pr (Fig. 11b). This distribution is consistent with the findings of the northern hemisphere geographic distribution, as discussed in the previous section; each of the three morphologies tends to occur and be concentrated in the same regions, and multiple morphologies are often seen within the same image (Figs. 2 and 5).

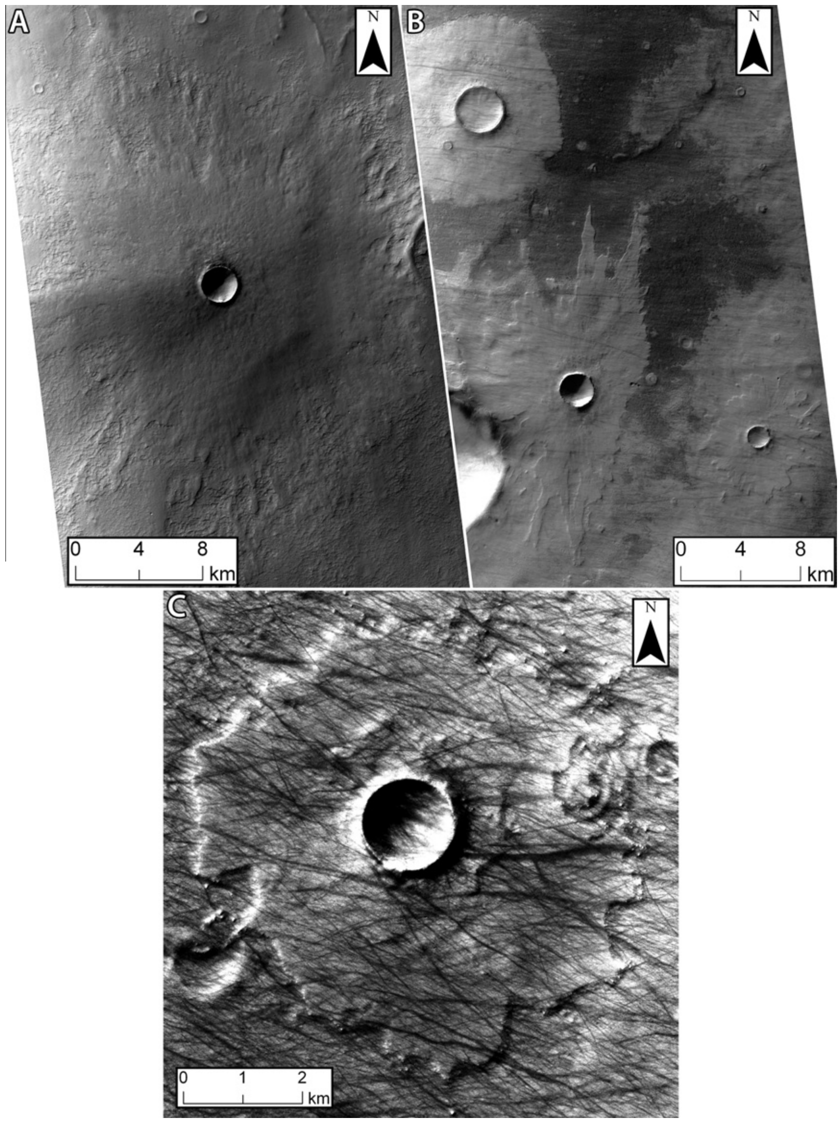

Fig. 11. Images of three of the newly identified excess ejecta craters in the southern hemisphere. Each example is less than 3 km in diameter, and exhibits DLE. (A) Crater #2 in Table 2, shown in CTX image P15_007030_1238. This crater has the largest ejecta area of the four EE identified in this study. The ejecta shows evidence of sublimation pitting, especially near the margins of its outer layer. (B) Crater #4 in Table 2, shown in CTX image P16_007264_1326. This EE is located within tens of km from two Pr, seen in the top left and bottom right of the image. The ejecta of this crater does show some signs of smoothing due to erosion, but it is notably fresher than that of the two Pr, and it maintains long lobes and radial striations. (C) Crater #1 in Table 2, shown in CTX image B11_013819_1162. Although this crater is still considered fresh, it shows the most abundant evidence of erosion of any of the new EE examples. Both layers of the DLE are visible, but the texture appears subdued.

Table 2
Locations and physical attributes of the four newly identified excess ejecta craters.

Crater #	Latitude (°S)	Longitude (°E)	Crater diam. (km)	Avg. ejecta thickness (m)	Ejecta area (km^2)	V_{cavity} (km^3)	V_{ejecta} (km^3)	V_{ejecta}/V_{cavity}
1	63.6	88.4	1.5	16	38	0.046	0.608	13.2
2	55.6	46.3	2.2	23	440	0.448	10.120	22.6
3	46.1	160.3	3.0	26	173	1.017	4.498	4.4
4	49.1	135.7	2.3	18	151	0.096	2.718	28.5

As noted in the Pd survey by Kadish et al. (2009), Pd are much more common in the northern hemisphere (Fig. 10). Our finding that both Pr and EE are also rarer in the southern hemisphere supports the interpretation that the morphologies are genetically related; having comparable relative population concentrations globally suggests that the crater types are similarly inhibited from forming in certain regions while other regions are conducive to the formation of each morphology. The lack of any identified large EE in the southern hemisphere is consistent with the finding by Kadish et al. (2010) that the pedestals of Pd are, on average, thinner (not as tall) in the southern hemisphere. In general, the smaller number of each morphologic crater type (EE, Pd, Pr), their geographic distribution (Fig. 10), and their thinner ejecta deposits/pedestals in the southern hemisphere imply that the ice-rich target material was less common in the southern highlands; specifically, these pieces of evidence support the interpretation that

Table 3
General comparison of the three crater morphologies.

	Excess ejecta craters	Perched craters	Pedestal craters
Typical crater diameter	5–18 km	3–23 km	<0.5–6 km
Typical ejecta/pedestal thickness	27–108 m, with a mean of ~50 m	35–140 m	20–110 m, with a mean of 46 m
Ejecta type/texture	Usually DLE with a rough rocky texture	SLE or DLE with a subdued rough texture	No ejecta or SLE with a smooth texture
Distribution	Tens of known examples, present at mid latitudes in both hemispheres	Hundreds of known examples, present at mid latitudes in both hemispheres	2300 + known examples, present at mid latitudes in both hemispheres
Age	Late Amazonian	Late Hesperian to Early Amazonian	Most are Late Amazonian, but some examples are Hesperian

the ice-rich paleodeposits in the southern hemisphere were thinner and not as geographically widespread. In other words, although southern hemisphere ice-rich deposits may have accumulated just as frequently as those in the northern hemisphere, the southern hemisphere deposits may not have reached the same thicknesses, may have sublimated more quickly, and/or may have been much more constrained to localized regions.

8. Discussion

The comparison of EE, Pr, and Pd yields some striking similarities as well as some key distinguishing traits (Table 3). This survey expands on the previous understanding of EE and Pr, both in terms of their geographic extents (Fig. 10) and physical sizes (Fig. 9). This information, in conjunction with prior detailed Pd studies, provides the necessary context from which we can draw a more comprehensive analysis of the potential relationship between these morphologies. In terms of physical size (Fig. 9), the survey does show that EE and Pr can occur at smaller diameters than found in previous measurements by Black and Stewart (2008) and Boyce et al. (2005). We measured one EE that was 1.5 km in diameter, and some of the Pd that are less than 2 km in diameter qualify as Pr. However, the majority of EE tend to be greater than 5 km, and the majority of Pr are greater than 3 km. We were unable to find any new examples of EE or Pr that exceeded the size of the largest examples identified by Black and Stewart (2008) and Boyce et al. (2005), respectively; nonetheless, their studies showed that both of these morphologies can reach approximately 20 km in diameter. Pd, on the other hand, can be much smaller, with many examples less than 1 km in diameter. In addition, Pd generally do not exceed 6 km.

If we combine this outline of the diameter ranges with the fact that each morphology exhibits almost identical excess ejecta/pedestal thicknesses (Fig. 3), with averages around 50 m in all cases, then the data suggest that morphologic variations are initially based on excavation depth relative to the thickness of the ice-rich target layer; each morphology protects/insulates the same layer thickness, but the size of the impactor (and possibly other characteristics including impact velocity, impact angle, and target material strength) determines the crater depth. If the impact penetrates through the ice-rich material and excavates regolith, it creates a significant ejecta deposit. If not, it can result in a smooth armored pedestal that has a minimal ejecta deposit, or lacks ejecta altogether (Fig. 8).

This interpretation is supported by both the geographic distribution and morphologic characteristics of EE, Pr, and Pd. Specifically, the fact that the morphologies are all located in the same geographic regions within the same restricted latitudinal bands in mid to high latitudes (Fig. 10) supports the interpretation that they all require the same target material, which appears to accumulate in response to a climate-related mechanism. Our expansion of the EE and Pr surveys into the southern hemisphere shows that they occur where Pd are present. This confirms that the highest concentrations of each crater type occur in the same regions in both hemispheres. What would cause the much larger population of Pd craters? Given the fact that smaller impacts occur more frequently based on the size–frequency distribution of the impactor population, one would expect that the Pd population would grow most rapidly during periods when the ice-rich material was emplaced.

From a morphological perspective, the smoothness of pedestal surfaces, and the fact that most lack ejecta, is consistent with induration of a flat paleodeposit. Most of the ejecta would have been icy material given the thickness of the ice-rich deposit and the shallow excavation depths of small impacts. This ice-rich ejecta would have sublimated when the intercrater terrain sublimated and deflated. Regarding EE and Pr, the presence of DLE, radial striations, and rough surface textures suggests the presence of rocky material included in the ejecta, which must have been sourced from the underlying regolith. This requires that the impacts penetrated through the entire icy surface layer.

The ages of these morphologies, with EE being necessarily young (Amazonian) and Pr being usually older (Late Hesperian to Early Amazonian) suggests a possible evolution from EE to Pr. These two morphologies are located in the same geographic regions, and have the same diameter size ranges and ejecta characteristics. There are also many more Pr than EE (Fig. 10). These data suggest that EE are able to maintain the ice-rich content in their ejecta for geologically long timescales, on the order of tens to hundreds of millions of years. As EE age and become degraded, their crater interiors become infilled, and they become Pr (Fig. 2). The absence of fresh Pr and degraded EE supports the interpretation that at least some EE transform into Pr as they are mantled and eroded. Pd, being primarily young but having some old examples, experience a unique age progression that involves erosion of the pedestal from the scarp back to the crater rim through sublimation pitting along the margin (Kadish et al., 2010).

9. Conclusions

This study establishes associations between three distinctive crater morphologies (Table 3) that were previously studied independently. Through the assessment of excess ejecta craters (Black and Stewart, 2008), perched craters (Boyce et al., 2005; Meresse et al., 2006), and pedestal craters (Arvidson et al., 1976; Barlow et al., 2000; Kadish et al., 2009), we have established significant evidence for a genetic relationship between the crater types. Our expansion of previous surveys reveals that EE and Pr are present in the southern hemisphere in the same geographic locations as Pd. We have also shown that, in rare cases, EE and Pd can be smaller than the examples identified by previous studies.

These new survey results, in conjunction with the direct comparison of each morphology, lead us to conclude that:

(1) EE and Pr are genetically related, and are likely to have formed from the same general mechanism – ejecta armoring of an icy substrate (Fig. 8). The primary difference between

these morphologies is simply that Pr have experienced post-impact modification and infilling, resulting in extremely shallow crater depths and subdued ejecta textures.

(2) Given the diameter ranges of EE and Pr (Fig. 9), and the estimated thickness of the mid-latitude ice-rich deposit during periods of high obliquity (tens to hundreds of meters), these impacts overwhelmed the ice-rich layer, penetrating to the underlying martian silicate regolith. This resulted in the excavation of rock that formed the blocky ejecta necessary to preserve the ice-rich deposits.

(3) The smaller size of Pd, and the significant differences from Pr and EE in topographic profile due to the absence of ejecta, requires that Pd result from a slightly different process. The fact that the pedestals of Pd have the same average thickness as the excess ejecta of EE and Pr (Fig. 9), and form in the same geographic regions (Fig. 10) implies that they result from impacts into the same type of ice-rich target material. However, Pd differ in that they do not penetrate through the icy surface layer, and thus do not generate a rocky silicate-rich ejecta covering. Instead, an indurated, dusty lag deposit appears to protect the underlying ice-rich material.

(4) The ages of EE, Pr, and Pd suggest that ice-rich material has been repeatedly deposited at mid latitudes in both hemispheres throughout the Amazonian. The geographic distribution of EE, Pr, and Pd, with significantly higher concentrations in the northern hemisphere (Fig. 10), suggests that the lowlands may be superposed more frequently by these ice-rich deposits. Stratigraphic, morphologic, and crater counting evidence supports the interpretation that there have been multiple generations of these crater populations. This would require the episodic emplacement of icy paleodeposits, which are likely to have accumulated and sublimated at mid latitudes due to obliquity-driven climate variations.

Acknowledgments

The authors would like to thank the HiRISE, CTX, and HRSC teams, without whom this study could not have been completed, as well as Sarah Stewart and one anonymous reviewer for their constructive comments that improved the quality of the manuscript. The authors are grateful for financial support from NASA Mars Data Analysis Program (MDAP) Grant NNX09A14GG to J.W.H.

References

Arvidson, R.E., Coradini, M., Carusi, A., Coradini, A., Fulchignoni, M., Federico, C., Funiciello, R., Salomone, M., 1976. Latitudinal variation of wind erosion of crater ejecta deposits on Mars. Icarus 27 (4), 503–516. doi:10.1016/0019-1035(76)90166-4.

Barlow, N.G., 2005. A new model for pedestal crater formation. Workshop on the Role of Volatiles and Atmospheres on Martian Impact Craters. LPI Contribution No. 1273, pp. 17–18.

Barlow, N.G. et al., 2000. Standardizing the nomenclature of martian impact crater ejecta morphologies. J. Geophys. Res. 105 (E11), 26733–26738.

Barlow, N.G., Koroshetz, J., Dohm, J.M., 2001. Variations in the onset diameter for martian layered ejecta morphologies and their implications for subsurface volatile reservoirs. Geophys. Res. Lett. 28 (16), 3095–3098.

Black, B.A., Stewart, S.T., 2008. Excess ejecta craters record episodic ice-rich layers at middle latitudes on Mars. J. Geophys. Res. 113, E02015. doi:10.1029/2007JE002888.

Boyce, J.M., Mouginis-Mark, P., 2006. Martian craters viewed by the Thermal Emission Imaging System instrument: Double-layered ejecta craters. J. Geophys. Res. 111, E10005. doi:10.1029/2005JE002638.

Boyce, J.M., Mouginis-Mark, P., Garbeil, H., 2005. Ancient oceans in the northern lowlands of Mars: Evidence from impact crater depth/diameter relationships. J. Geophys. Res. 110, E03008. doi:10.1029/2004JE002328.

Forget, F., Haberle, R.M., Montmessin, F., Levrard, B., Head, J.W., 2006. Formation of glaciers on Mars by atmospheric precipitation at high obliquity. Science 311, 368–371.

Garvin, J.B., Sakimoto, S.E.H., Frawley, J.J., Schnetzler, C., 2000. North polar region craterforms on Mars: Geometric characteristics from the Mars Orbiter Laser Altimeter. Icarus 144, 329–352.

Garvin, J.B., Sakimoto, S.E.H., Frawley, J.J., 2003. Craters on Mars: Global geometric properties from gridded MOLA topography. In: Sixth International Conference on Mars. Abstract #3277.

Head, J.W., Marchant, D.R., 2003. Cold-based mountain glaciers on Mars: Western Arsia Mons. Geology 31, 641–644. doi:10.1130/0091-7613.

Head, J.W., Marchant, D.R., 2009. Inventory of ice-related deposits on Mars: Evidence for burial and long-term sequestration of ice in non-polar regions and implications for the water budget and climate evolution. Lunar Planet. Sci. XL. Abstract #1356.

Head, J.W., Mustard, J.F., Kreslavsky, M.A., Milliken, R.E., Marchant, D.R., 2003. Recent ice ages on Mars. Nature 426, 797–802.

Kadish, S.J., Head, J.W., 2011. Preservation of layered paleodeposits in high-latitude pedestal craters on Mars. Icarus 213 (2), 443–450. doi:10.1016/j.icarus.2011.03.029.

Kadish, S.J., Head, J.W., Barlow, N.G., Marchant, D.R., 2008. Martian pedestal craters: Marginal sublimation pits implicate a climate-related formation mechanism. Geophys. Res. Lett. 35, L16104. doi:10.1029/2008GL034990.

Kadish, S.J., Barlow, N.G., Head, J.W., 2009. Latitude dependence of martian pedestal craters: Evidence for a sublimation-driven formation mechanism. J. Geophys. Res. 114, E10001. doi:10.1029/2008JE003318.

Kadish, S.J., Head, J.W., Barlow, N.G., 2010. Pedestal crater heights on Mars: A proxy for the thicknesses of past, ice-rich, Amazonian deposits. Icarus 210, 92–101. doi:10.1016/j.icarus.2010.06.021.

Kreslavsky, M., Head, J.W., 2002. Mars: Nature and evolution of young latitude-dependent water-ice-rich mantle. Geophys. Res. Lett. 29. doi:10.1029/2002GL015392.

Laskar, J., Correia, A.C.M., Gastineau, M., Joutel, F., Levrard, B., Robutel, P., 2004. Long term evolution and chaotic diffusion of the insolation quantities of Mars. Icarus 170 (2), 343–364.

Lefort, A., Russell, P., Thomas, N., McEwen, A., Dundas, C.M., Kirk, R., 2009. Observations of periglacial landforms in Utopia Planitia with the High Resolution Imaging Science Experiment (HiRISE). J. Geophys. Res. 114. doi:10.1029/2008JE003264.

Levrard, B., Forget, F., Montmessin, F., Laskar, J., 2004. Recent ice-rich deposits formed at high latitudes on Mars by sublimation of unstable equatorial ice during low obliquity. Nature 431, 1072–1075.

Levy, J., Head, J.W., Marchant, D.R., 2010. Concentric crater fill in the northern mid-latitudes of Mars: Formation processes and relationships to similar landforms of glacial origin. Icarus 209, 390–404. doi:10.1016/j.icarus.2010.03.036.

Madeleine, J.-B., Forget, F., Head, J.W., Levrard, B., Montmessin, F., Millour, E., 2009. Amazonian northern mid-latitude glaciation on Mars: A proposed climate scenario. Icarus 203, 390–405.

McCauley, J.F., 1973. Mariner 9 evidence for wind erosion in the equatorial and mid-latitude regions of Mars. J. Geophys. Res. 78, 4123–4137. doi:10.1029/JB078i020p04123.

Melosh, H.J., 1989. Impact Cratering: A Geological Process. Oxford Univ. Press, New York.

Meresse, S., Costard, F., Mangold, N., Baratoux, D., Boyce, J.M., 2006. Martian perched craters and large ejecta volume: Evidence for episodes of deflation in the northern lowlands. Meteorit. Planet. Sci. 41, 1647–1658.

Morgan, G.A., Head, J.W., 2009. Sinton crater, Mars: Evidence for impact into a plateau icefield and melting to produce valley networks at the Hesperian–Amazonian boundary. Icarus 202, 39–59.

Mustard, J.F., Cooper, C.D., Rifkin, M.K., 2001. Evidence for recent climate change on Mars from the identification of youthful near-surface ground ice. Nature 412, 411–414.

Osinski, G.R., 2006. Effect of volatiles and target lithology on the generation and emplacement of impact crater fill and ejecta deposits on Mars. Meteorit. Planet. Sci. 41 (10), 1571–1586.

Schaefer, E.I., Head, J.W., Kadish, S.J., 2011. Vaduz, an unusual fresh crater on Mars: Evidence for impact into a recent ice-rich mantle. Geophys. Res. Lett. 38, L07201. doi:10.1029/2010GL046605.

Schultz, P.H., Mustard, J.F., 2004. Impact melts and glasses on Mars. J. Geophys. Res. 109. doi:10.1029/2002JE002025.

Skorov, Y.V., Markiewicz, W.J., Basilevsky, A.T., Keller, H.U., 2001. Stability of water ice under a porous nonvolatile layer: Implications to the south polar layered deposits of Mars. Planet. Space Sci. 49, 59–63. doi:10.1016/S0032-0633(00)00121-5.

Smith, D.E. et al., 2001. Mars orbiter laser altimeter: Experiment summary after the first year of global mapping of Mars. J. Geophys. Res. 106. doi:10.1029/2000JE001364.

Stewart, S.T., Valiant, G.J., 2006. Martian subsurface properties and crater formation processes inferred from fresh impact crater geometries. Meteorit. Planet. Sci. 41, 1509–1537.

Wrobel, K., Schultz, P., Crawford, D., 2006. An atmospheric blast/thermal model for the formation of high-latitude pedestal craters. Meteorit. Planet. Sci. 41 (10), 1539–1550.